The Astrophysical Journal Supplement Series, 154:97–102, 2004 September

DEEP MID-INFRARED OBSERVATIONS OF LYMAN BREAK GALAXIES

P. Barmby,[1] J.-S. Huang,[1] G. G. Fazio,[1] J. A. Surace,[2] R. G. Arendt,[3] J. L. Hora,[1] M. A. Pahre,[1] K. L. Adelberger,[4] P. Eisenhardt,[5] D. K. Erb,[6] M. Pettini,[7] W. T. Reach,[2] N. A. Reddy,[6] A. E. Shapley,[8] C. C. Steidel,[6] D. Stern,[5] Z. Wang,[1] and S. P. Willner[1]

Received 2004 March 26; accepted 2004 May 7

ABSTRACT

As part of the in-orbit checkout activities for the *Spitzer Space Telescope*, the Infrared Array Camera (IRAC) team carried out a deep observation (average integration time ~8 hr) of a field surrounding the bright QSO HS 1700+6416. This field contains several hundred $z \sim 3$ Lyman break galaxy (LBG) candidates, and we report here on their mid-infrared properties, including the IRAC detection rate, flux densities, and colors, and the results of fitting population synthesis models to the optical, near-infrared, and IRAC magnitudes. The results of the model fitting show that previous optical/near-infrared studies of LBGs were not missing large, hidden old stellar populations. The LBG candidates' properties are consistent with those of massive star-forming galaxies at $z \sim 3$. Other IRAC sources in the same field have similar properties, so IRAC selection may prove to be a promising method of finding additional high-redshift galaxies.

Subject headings: galaxies: high-redshift — galaxies: stellar content — infrared: galaxies

1. INTRODUCTION

Observations of galaxies at high redshift provide important tests of theories of galaxy and structure formation: galaxy masses, star formation rates, and the distribution of these quantities are all vital information. Some of the best-known high-redshift galaxies are the $z \sim 3$ galaxies discovered with the Lyman break technique (Steidel & Hamilton 1993). These galaxies are forming stars rapidly and are generally thought to be massive enough to be the ancestors of today's large galaxies (Adelberger et al. 1998; Steidel et al. 1998; Weatherley & Warren 2003). Rest-frame near-infrared observations primarily sample the old stellar population in galaxies and are not severely affected by dust extinction. They should provide a less-biased estimator of the galaxy mass than optical measurements, which are sensitive to both internal extinction and emission from young stars that make up little of the galaxy mass (Brinchmann & Ellis 2000; Kauffmann & Charlot 1998). The four bands of the Infrared Array Camera (IRAC; Fazio et al. 2004a) on the *Spitzer Space Telescope* (Werner et al. 2004) probe the rest-frame near-infrared at redshifts $z = 2$–4.

This paper reports *Spitzer* IRAC 3–10 μm observations of a Lyman break galaxy (LBG) field. The goals of the observations were to confirm that IRAC could detect $z \sim 3$ galaxies and to characterize the noise performance in the approach to the confusion limit. Galaxy number counts in this field are addressed in a separate paper (Fazio et al. 2004b). IRAC properties of $z \sim 2$ galaxies in this field are also addressed in a separate paper (C. C. Steidel et al. 2004, in preparation). Throughout this paper we assume a cosmology with $H_0 = 70$ km s^{-1} Mpc^{-1}, $\Omega_m = 0.3$, and $\Omega_\Lambda = 0.7$.

2. OBSERVATIONS AND DATA REDUCTION

The field observed was an LBG field surrounding the $z = 2.7$ QSO HS 1700+6416, from the survey of Steidel et al. (2004). This particular field was chosen because of its existing very deep optical photometry, which allowed selection of high-redshift galaxies, and its position within the *Spitzer* continuous viewing zone. The field also includes two galaxy clusters (A2246 at $z = 0.25$ and an anonymous cluster at $z = 0.44$) whose X-ray emission was discovered during a study of the QSO (Reimers et al. 1997). The IRAC observations were centered at coordinates $\alpha = 17^{\rm h}01^{\rm m}17^{\rm s}$, $\delta = 64^\circ09'02''$ (J2000.0), ~3.′7 southeast of the QSO. The central IRAC pointing was offset in order to slightly lower the observed galaxy density and reduce the effects of confusion. The two IRAC fields of view see different regions of the sky, so the final 3.6 and 5.8 μm images extend further to the southeast while the 4.5 and 8.0 μm images extend to the northwest. The IRAC images were taken on (UT) 2003 October 14–16 as part of *Spitzer* Program ID (PID) 620. We used 200 s frame times in the 3.6–5.8 μm channels; this observing mode uses 50 s frame times in the 8.0 μm band because of the higher sky background. We obtained some additional data with 100 s frame times, but only used the 8.0 μm band data (which again uses 50 s frame times) to avoid systematics in combining data taken with different frame times.

The individual images were processed with the *Spitzer* Science Center (SSC) pipeline, then had their astrometric positions refined with Two Micron All Sky Survey (2MASS) sources. The zero levels of the 5.8 μm band images were adjusted to minimize differences in the overlap areas using the overlap consistency option in the SSC processing tools. The images were combined into mosaics with our IDL-based code, which reprojected the images to correct for distortion and

[1] Harvard-Smithsonian Center for Astrophysics, 60 Garden Street, Cambridge, MA 02138; pbarmby@cfa.harvard.edu.
[2] *Spitzer* Science Center, MC 220-6, California Institute of Technology, Pasadena, CA 91125.
[3] Science Systems and Applications, Inc., Code 685, NASA Goddard Space Flight Center, Greenbelt, MD 20771.
[4] Observatories of the Carnegie Institution of Washington, 813 Santa Barbara Street, Pasadena, CA 91101.
[5] Jet Propulsion Laboratory, California Institute of Technology, MC 169-327, Pasadena, CA 91109.
[6] California Institute of Technology, MC 105-24, Pasadena, CA 91125.
[7] Institute of Astronomy, Madingley Road, Cambridge CB3 0HA, UK.
[8] Astronomy Department, 601 Campbell Hall, University of California, Berkeley, CA 84720.

combined them with a sigma-clipping algorithm. The resulting mosaics are in the original array orientation, with a pixel scale half as large as the original.[9]

Figure 1 (Plate 1) shows portions of the central regions of the mosaic images in the four IRAC bands. Because of dithering, the effective exposure time across the mosaics varies, ranging from ~11 hr in the deepest areas to 20 minutes near the edges. The average exposure time over the central $5' \times 10'$ area is 7.8 hr. The detection limits vary with the effective exposure time; approximate 5 σ limits in the central regions of the images are 0.45, 0.45, 0.8, and 0.9 μJy (AB magnitudes of 25.0, 25.0, 24.2, 24.1, respectively) in the four bands.

The optical data used for LBG selection are described by Steidel et al. (2004). Although these data were obtained for a survey of $z = 2$ galaxies, the imaging methods are the same for both the $z = 2$ and $z = 3$ selection (only the color criteria differ). Briefly, the optical imaging observations were obtained at the William Herschel 4.2 m telescope in 2001 May and supplemented with U-band images from Keck I/LRIS-B later that year for the central region near the QSO. The 1 σ surface brightness limits in the three bands (in a $1''$ aperture) are $U_n(\mathrm{AB}) = 28.9$, $G(\mathrm{AB}) = 29.0$, and $R_s(\mathrm{AB}) = 28.2$. A deep K_s-band image with $K_{\mathrm{AB}} = 23.9(5\ \sigma)$ covering the central $9' \times 9'$ was obtained at the Palomar Hale Telescope in 2003 June. Optical spectroscopy of an LRIS-B mask targeting 22 $z \sim 3$ candidates was obtained in 2003 September. Reduction followed the method described by Steidel et al. (2003), and 17 redshifts were successfully measured, with $\bar{z} = 2.911$. The spectroscopically confirmed galaxies had a median $R_s(\mathrm{AB}) = 24.6$.

3. ANALYSIS

3.1. *Object Detection and Photometry*

LBG selection was done using the $U_nG\mathcal{R}$ technique described by Steidel et al. (2003). A total of 445 LBG candidates in the $15' \times 15'$ area centered on the QSO were selected, to a limiting total magnitude of $R_s(\mathrm{AB}) = 25.5$. These objects are typically >10 σ detections in $\mathcal{R}$, 15–20 σ in G, and very faint or undetected in U_n. In general, spectroscopic observations of LBG candidates show that ~95% are likely to be bona fide $z \approx 3$ galaxies (Steidel et al. 2003). There are about 110 LBG candidates in the 3.6 μm/5.8 μm field of view, ~175 candidates in the 4.5 μm/8.0 μm field of view, and ~90 in the overlap area. Parts of the final 3.6 and 5.8 μm images extend outside the $U_nG\mathcal{R}$ detection images.

To detect LBG candidates on the IRAC images, we used the image world coordinate system to project the candidates' positions into the image plane and performed aperture photometry at those positions. We experimented with allowing the photometry algorithm to recenter the objects; if the objects moved more than $1''.2$ in either x or y (indicating that the identification was in danger of moving to a nearby object), we used the uncentered position. This is important because the IRAC images are crowded, particularly at the shorter wavelengths (the IRAC point-spread function [PSF] FWHM is ~$1''.8$–$2''.0$). As an indicator of detection significance, we used the IRAF/APPHOT photometric uncertainty inside a $1''.5$ radius aperture, with sky counts determined in $15''$–$20''$ annuli. Objects with magnitude uncertainty less than 0.217 mag (S/N > 5) were considered detected (see Fig. 1 for examples). The final IRAC detection numbers for the four bands are given in Table 1. Most of the LBG candidates were detected at 3.6 and 4.5 μm; the detection rate decreases with increasing wavelength to 45% at 8.0 μm. Photometry of the LBG candidates was completed by applying aperture corrections from the $1''.5$ measurement aperture to the $12''.2$ aperture used for flux calibration. The corrections, derived from the measured IRAC PSF (S. T. Megeath 2004, private communication), are −0.52, −0.55, −0.74, and −0.85 mag.

TABLE 1
IRAC Detections of Lyman Break Galaxies

IRAC Band	Photometric Candidates		Confirmed $z \sim 3$	
	$N(U_nG\mathcal{R})$[a]	N(IRAC)[b]	N(LRIS)[a]	N(IRAC)[b]
3.6 μm	114	104	14	14
4.5 μm	180	150	10	10
5.8 μm	112	68	16	14
8.0 μm	170	77	10	7

[a] Number in field.
[b] Number detected with IRAC.

To generate a sample of IRAC-selected non-LBG objects for comparison to the LBG candidates, we used DAOFIND to find objects to a threshold of 5 σ above local background. The detection images were the IRAC mosaics multiplied by the square root of the coverage maps (to give uniform noise across the images) with areas near the image edges, near bright stars, or near instrumental artifacts masked out. Detection was performed in the 3.6 and 4.5 μm band images only, with object positions transferred to the frame of the 5.8 and 8.0 μm band images for photometry. For a more reliable sample, we included only objects detected in both 3.6 and 4.5 μm bands, which restricts the area used to ~42 arcmin^2. About half of the LBG candidates in the field were detected as part of this sample (the rest were too close to brighter objects or masked areas), and were removed. The final non-LBG sample contained 1931 objects. Photometry of the non-LBG sample was done in an identical manner to that of the LBG candidates. No attempt was made to separate stars and galaxies in the non-LBG sample on the basis of spatial extent; the size of the IRAC PSF makes this impractical for distant galaxies. The Galactic coordinates of the field ($l = 94^\circ.3, b = +36^\circ.2$) are such that we do not expect stellar contamination to be a serious problem for faint objects.

3.2. *LBG Properties: Flux and Color Distributions*

To compare the optical properties of IRAC-detected and nondetected LBGs we used the optical catalog generated for LBG selection. There was no significant difference (K-S test probability >5%) in $\mathcal{R}$ between objects detected and not detected in the 3.6 μm band. However, there are so few nondetections in this band (only 10) that this comparison is not particularly meaningful. A K-S test of the $\mathcal{R}$-magnitude distributions of IRAC detections and nondetections in the 4.5, 5.8, and 8.0 μm bands showed that the differences in mean magnitudes are statistically significant. The IRAC-detected objects are roughly 0.2–0.4 mag brighter in $\mathcal{R}$ than the nondetected objects. There is, however, no clear correlation between $\mathcal{R}$ and IRAC magnitudes for the IRAC-detected objects.

We can also compare the IRAC flux density distributions of the LBG candidates and the non-LBG sample. The LBGs have

[9] The mosaics are available at http://cfa-www.harvard.edu/irac/publications. Links to the data from this paper, *Spitzer* AOR keys 0007127552, 0007127808, 0007128064, 0007128320, 0007128576, 0007475968, 0007476224, and 0007476480 are available through the electronic edition.

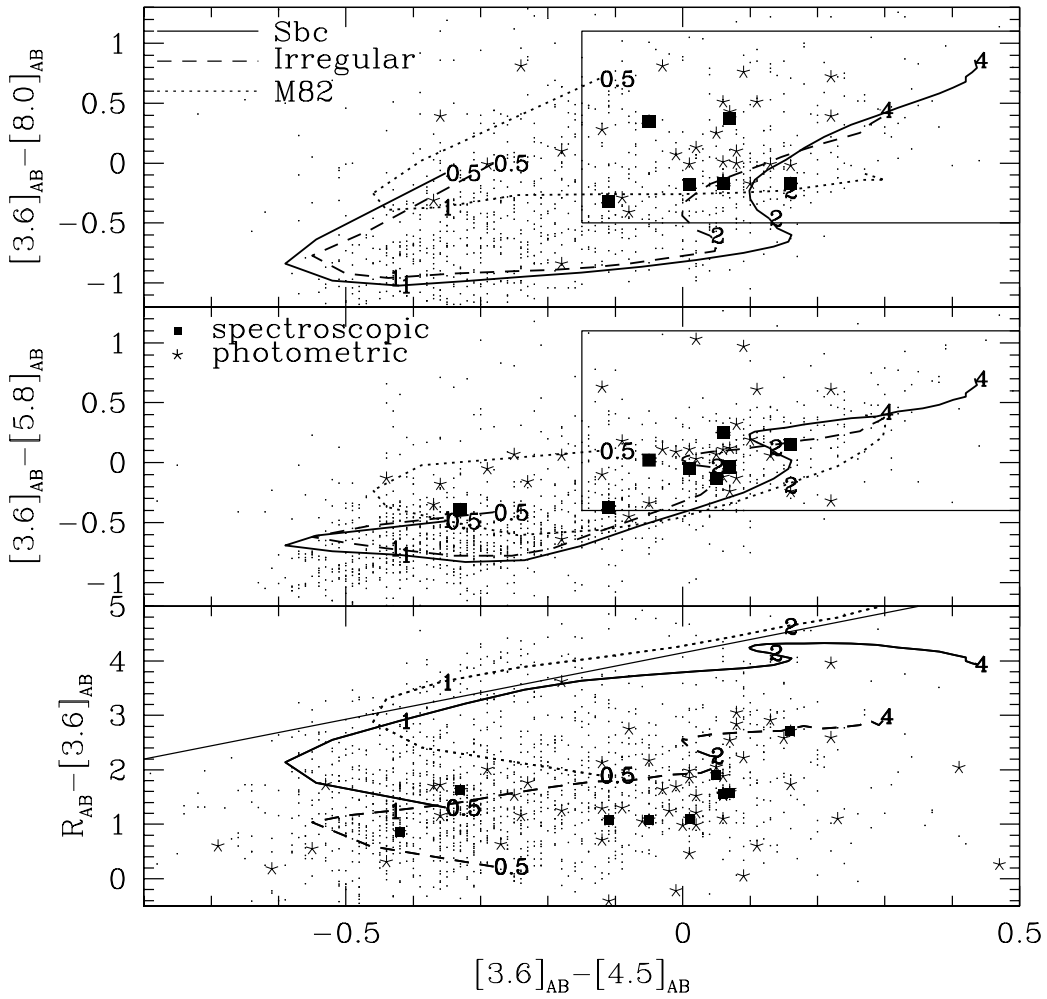

FIG. 2.—Two-color plots of LBG candidates (*asterisks*), confirmed $z \sim 3$ LBGs (*filled squares*), and the non-LBG sample (*dots*). Lines are template SEDs for $0.5 < z < 4$, with redshifts 0.5, 1, 2, and 4 marked. The different templates are Sbc spiral (*thick solid line*), irregular (*dashed line*), and M82 (*dotted*). Thin solid lines indicate color-selection criteria for high-redshift galaxies.

median IRAC magnitudes 0.5–0.7 fainter than the non-LBG sample. The spectroscopically confirmed galaxies are slightly brighter than the full candidate list in the 3.6 and 4.5 μm bands and slightly fainter in the longer wavelength bands (but their numbers are small: only six such galaxies have four IRAC-band detections). The 33 LBG candidates detected in all four IRAC bands have median AB magnitudes in the IRAC bands of 22.7, 22.7, 22.6 and 22.5 (flux densities in μJy: 3.1, 3.1, 3.3, 3.8, respectively). Two-color plots are shown in Figure 2. The LBGs are redder than the comparison objects in [3.6]–[4.5], for which the color limit is constant with magnitude. Selection effects bias the observed color distributions in [3.6]–[5.8] and [3.6]–[8.0]: because of the different sensitivities in the IRAC bands, bluer objects are observable only at bright [3.6] magnitudes.

Figure 2 also shows predicted colors for template SEDs. The templates combine optical and near-infrared data from the HYPERZ package (Bolzonella et al. 2000) and mid-infrared data from Lu et al. (2003). As Papovich et al. (2001) report for optical/near-infrared data, the "irregular galaxy" template SED is the closest match to the LBG candidates' colors, particularly the spectroscopically confirmed objects. Besides being known to be at the correct redshift, the spectroscopic galaxies also tend to be brighter, so their colors should be better determined. A substantial number of LBG candidates fall well away from the template colors, which could happen for several reasons: photometric error (e.g., due to contamination by nearby objects) or incomplete or inapplicable templates.

Some objects in the comparison sample have the same fluxes and colors as the LBG candidates, and therefore could be high-redshift galaxies. Using the top two panels of Figure 2, we suggest selection criteria for $z > 2$ galaxies based on both the LBG candidate observations and the template tracks. The criteria $[3.6]_{AB}-[4.5]_{AB} > -0.15$, $1.1 > [3.6]_{AB}-[5.8]_{AB} > -0.4$, $1.1 > [3.6]_{AB}-[8.0]_{AB} > -0.5$, and $[3.6]_{AB} > 22$ give good separation between low and high-redshift galaxy templates, while including about 2/3 of the LBG candidates and all but one spectroscopically confirmed LBG. This color criterion would also pick up some M82-like SEDs at $1 < z < 2$; however, the bottom panel of the figure shows that adding the criterion $R_{AB}-[3.6] < 4.1 + 2.4([3.6]_{AB}-[4.5]_{AB})$ should reduce the number of such objects. These criteria define a subsample of 86 objects from the non-LBG sample, giving an areal density of approximately 2 arcmin^{-2}. This is comparable to the number density of LBGs in the same area (2.0 arcmin^{-2}). While the LBG technique is designed to select galaxies over a fairly narrow redshift range, the use of IRAC/optical colors may permit selection of high-z galaxies without biases toward UV-bright objects, albeit with an as yet undetermined

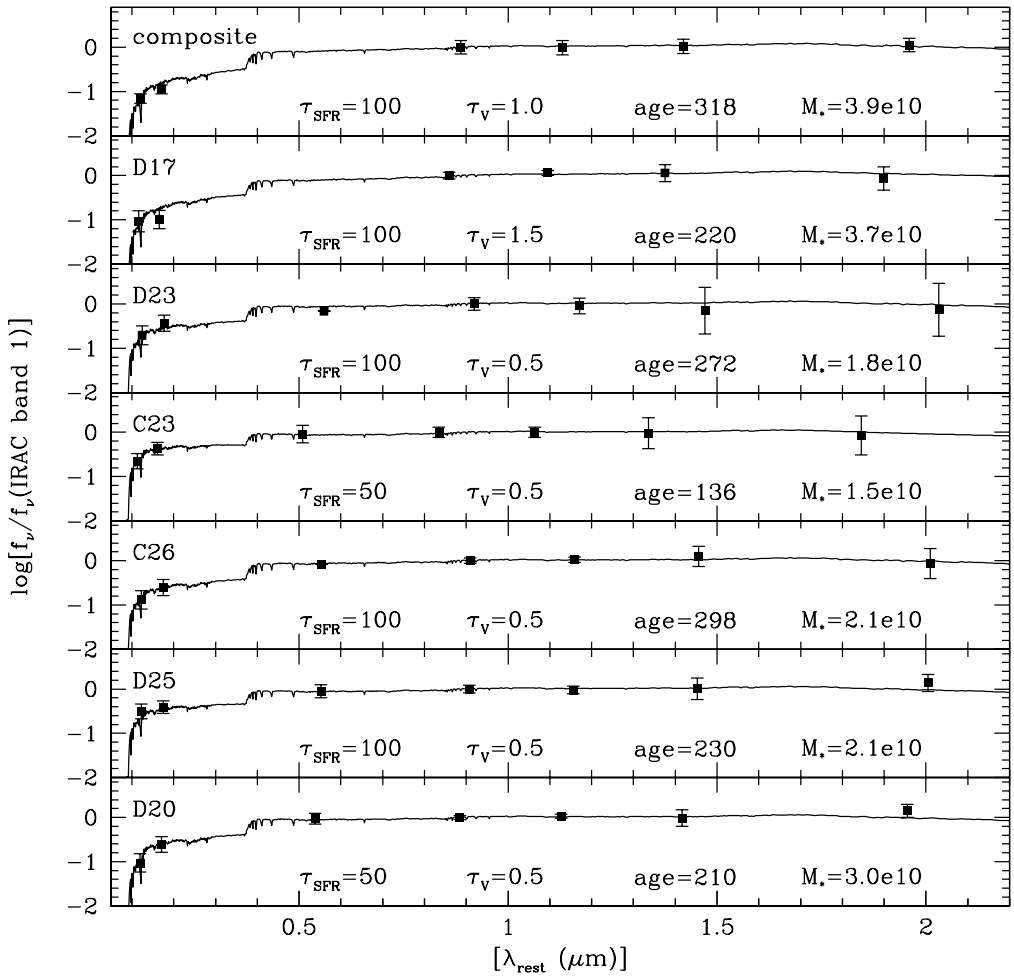

FIG. 3.—SEDs for spectroscopically confirmed LBGs and a composite of the photometric candidates. Low-resolution SEDs for the best-fitting Bruzual & Charlot (2003) models are shown; models are normalized to the data at $\lambda_{obs} = 3.6$ μm ($\lambda_{rest} \approx 0.9$ μm). From shortest to longest wavelength, the photometric points marked are in the G, $\mathcal{R}$, K_s, 3.6, 4.5, 5.8, and 8.0 μm bands. Ages and τ_{SFR} are in Myr; stellar masses are in $M_\odot$.

contamination rate (see also Huang et al. 2004). Confirmation of such color selection with spectroscopic redshifts is of course necessary, and this will be the subject of future investigations.

3.3. *Spectral Energy Distributions and Model Fitting*

At high redshifts, the IRAC bands sample the rest-frame near-IR light of galaxies. This light is expected to be a good tracer of galaxy stellar mass since it comes mainly from low-mass older stars. To test this assumption, we compared stellar population synthesis to the combination of optical, near-infrared, and IRAC data. Following Shapley et al. (2001), we used the population synthesis models of Bruzual & Charlot (2003) to generate synthetic spectral energy distributions (SEDs) for composite stellar populations with solar metallicity, a Salpeter (1955) initial mass function, and star formation rates (SFRs)

$$\Psi(t) = \Psi_0 e^{-t/\tau_{SFR}}, \quad (1)$$

with $\tau_{SFR} = 10, 50, 100$ Myr, and galaxy ages at $z = 3$ of 10, 50, 100, 200, 500, 1000, 1200, 1500 and 2000 Myr, corresponding to formation redshifts $3.21 < z_f < 30$. As a matter of convenience, we used the Bruzual & Charlot (2003) code's internal prescription for extinction, derived from Charlot & Fall (2000). Models with four different values of the extinction parameter τ_V (0.5, 0.75, 1.0, 1.5) were generated. Predictions for observed fluxes were made from the model SEDs using the program CM_EVOLUTION included in Bruzual & Charlot's software distribution. We expect the rest-frame UV photometry to provide a more sensitive estimate of the instantaneous SFR in these models, while the rest-frame near-IR photometry from IRAC will provide the constraints on the integrated stellar mass.

The best-fitting models were determined by minimizing χ^2, the sum of the difference between model and observations. The Bruzual & Charlot (2003) models have a tabulated stellar mass for each age, so the overall best-fit normalization of the model apparent magnitudes fixes the model stellar mass. We fit models to the GRK_s + IRAC magnitudes of each of the six spectroscopically confirmed galaxies individually and to a "composite" SED made from the median fluxes of the 26 unconfirmed candidates (assumed to be at $z = 3.00$). The model SEDs and observations, with model parameters, are shown in Figure 3. Current star formation rates $\Psi(t_{obs})$ are derived using equation (1) and requiring $\int_0^{t_{obs}} \Psi(t)\,dt = (1 - R)M_*$ ($R = 0.28$ is the fraction of formed stellar mass returned to the interstellar medium; Cole et al. 2000).

Most of the observations are best fit by models with star formation $\tau_{SFR} = 50$–100 Myr, relatively young ages (100–300 Myr), and stellar masses in the range 1.5–4×10^{10} $M_\odot$.

The resulting SFRs are 7–33 $M_\odot$ yr^{-1}. The largest SFR is for D17, a galaxy without a measured K_s-band magnitude that also has a large best-fit extinction. This object has bluer IRAC colors than the predicted SED of the prototype dusty starburst M82 but could be intermediate in type between M82 and a nearby irregular. Previous results on SED fitting of LBGs with optical and near-infrared observations are presented by Shapley et al. (2001) and Papovich et al. (2001); the latter used a much more extensive grid of population synthesis models. Our model parameters are well within the range of best-fit parameters found by these two groups, indicating that IRAC-detected LBGs are not particularly unusual members of the LBG population, and the previous optical/near-infrared studies were not missing large, hidden old stellar populations. More sophisticated model fitting, using a wider range of stellar population parameters and extinction prescriptions, is clearly possible, but beyond the scope of this paper. Such analysis will be pursued in subsequent work, using these data and a larger sample of LBGs in the extended Groth strip survey area.

4. SUMMARY

Deep observations with IRAC detect nearly all $R_{\rm AB} < 25.5$ Lyman break galaxy candidates at 3.6 and 4.5 μm, and about half of the candidates at 5.8 and 8.0 μm. The color and magnitude distributions of LBGs overlap with those of a sample of comparison objects in the IRAC field. This suggests that IRAC selection may allow detection of different types of high-redshift galaxies than are found by Lyman break selection. SED fitting implies that the IRAC-detected LBGs are massive stellar systems with relatively recent star formation. The sensitivity of IRAC to old stellar light at these high redshifts shows its promise for future work in galaxy formation and evolution.

We thank M. Ashby for a careful reading of the manuscript, and the referee for helpful comments. This work is based on observations made with the *Spitzer Space Telescope*, which is operated by the Jet Propulsion Laboratory, California Institute of Technology under NASA contract 1407. Support for this work was provided by NASA through contract 1256790 issued by JPL/Caltech. Support for the IRAC instrument was provided by NASA through contract 960541 issued by JPL. M. A. P. acknowledges NASA/LTSA grant NAG5-10777.

REFERENCES

Adelberger, K. L., Steidel, C. C., Dickinson, M., Giavalisco, M., Pettini, M., & Kellogg, M. 1998, ApJ, 505, 18
Bolzonella, M., Miralles, J.-M., & Pelló, R. 2000, A&A, 363, 476
Brinchmann, J., & Ellis, R. S. 2000, ApJ, 536, L77
Bruzual, G., & Charlot, S. 2003, MNRAS, 344, 1000
Charlot, S., & Fall, S. M. 2000, ApJ, 539, 718
Cole, S., Lacey, C. G., Baugh, C. M., & Frenk, C. S. 2000, MNRAS, 319, 168
Fazio, G. G., et al. 2004a, ApJS, 154, 10
———. 2004b, ApJS, 154, 39
Huang, J.-S., et al. 2004, ApJS, 154, 44
Kauffmann, G., & Charlot, S. 1998, MNRAS, 297, L23
Lu, N., et al. 2003, ApJ, 588, 199
Papovich, C., Dickinson, M., & Ferguson, H. C. 2001, ApJ, 559, 620
Reimers, D., Toussaint, F., Hagen, H.-J., Hippelein, H., & Meisenheimer, K. 1997, A&A, 326, 489
Salpeter, E. E. 1955, ApJ, 121, 161
Shapley, A. E., Steidel, C. C., Adelberger, K. L., Pettini, M., Dickinson, M., & Giavalisco, M. 2001, ApJ, 562, 95
Steidel, C. C., Adelberger, K. L., Dickinson, M., Giavalisco, M., Pettini, M., & Kellogg, M. 1998, ApJ, 492, 428
Steidel, C. C., Adelberger, K. L., Shapley, A. E., Pettini, M., Dickinson, M., & Giavalisco, M. 2003, ApJ, 592, 728
Steidel, C. C., & Hamilton, D. 1993, AJ, 105, 2017
Steidel, C. C., Shapley, A. E., Pettini, M., Adelberger, K. L., Erb, D. K., Reddy, N. A., & Hunt, M. P. 2004, ApJ, 604, 534
Weatherley, S. J., & Warren, S. J. 2003, MNRAS, 345, L29
Werner, M. W., et al. 2004, ApJS, 154, 1

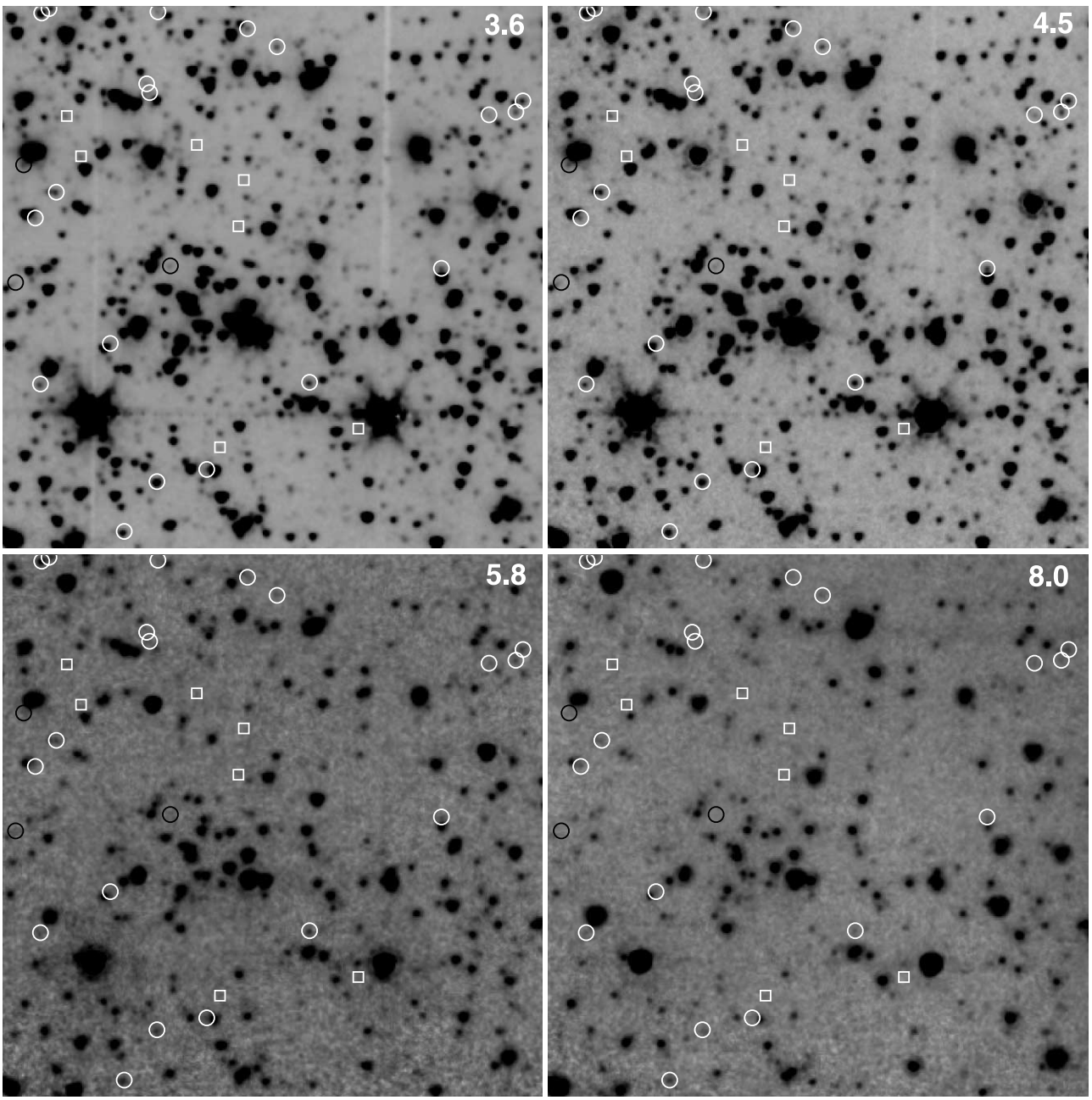

FIG. 1.—IRAC images of the Q1700+64 field in the four bands (wavelength labels are in the upper right of the images). These images show a portion ($3.'5 \times 3.'5$) of the area covered by all four IRAC bands; north is to the upper right and east to the upper left. White circles indicate LBGs detected in all four IRAC bands; black circles are LBGs detected in three bands; white squares are LBGs detected in two bands.